Determination of the heat diffusion anisotropy by comparing measured and simulated electron temperature profiles across magnetic islands

M. Hölzl[1], S. Günter[1], I. G. J. Classen[1,2], Q. Yu[1], the TEXTOR Team[3], and E. Delabie[2]

[1]*Max-Planck-Institut für Plasmaphysik, EURATOM Association, Boltzmannstraße 2, 85748 Garching, Germany*

[2]*FOM-Institute for Plasma Physics Rijnhuizen, Association EURATOM-FOM, Trilateral Euregio Cluster, PO Box 1207, 3430 BE Nieuwegein, The Netherlands, www.rijnhuizen.nl*

[3]*Institut für Energieforschung-Plasmaphysik, Forschungszentrum Jülich GmbH, EURATOM Association, Trilateral Euregio Cluster, 52425 Jülich, Germany*

Abstract

The ratio between the heat diffusion coefficients parallel and perpendicular to the magnetic field lines, $\chi_{||}/\chi_{\perp}$, influences the flattening of the temperature profile inside magnetic islands and the driving term of neoclassical tearing modes [R. Fitzpatrick. Phys. Plasmas **2**, 825 (1995)]. The value of this anisotropy is, however, not easily accessible experimentally. This article presents a method to determine it from a systematic comparison of temperature measurements at magnetic islands to numerical heat diffusion simulations. The application of the method is demonstrated for a $2/1$ magnetic island in the TEXTOR tokamak, where a heat diffusion anisotropy of 10^8 is observed. This is lower by a factor of 40 than predicted by Spitzer and Härm [L. Spitzer and R. Härm. Phys. Rev. **89**, 997 (1953)] and a strong indication that the heat flux limit determines the flattening of the electron temperature across magnetic islands.

PACS numbers: 52.55.Dy, 52.25.Fi, 52.25.Xz

1. Introduction

Heat transport in magnetised plasmas is faster along magnetic field lines than perpendicular to them by many orders of magnitude [1], which brings about constant temperatures within each of the nested magnetic flux surfaces of tokamak equilibria and an experimentally observable flattening of the temperature profile inside magnetic islands [2]. A magnetic island consists of locally nested magnetic flux surfaces that may form by field line reconnection in response to an internal or external resonant magnetic perturbation at equilibrium flux surfaces where the safety factor q is rational. As magnetic field lines wind helically around an island on these island flux surfaces, a parallel contribution to the radial heat transport arises. A so-called heat conduction layer forms around the island separatrix through which the heat is transported across the magnetic island chain. The width of the heat conduction layer and the degree of flattening depend on the ratio between the island width, w, and the critical island width for temperature flattening [2],

$$w_c = \left(\frac{\chi_{||}}{\chi_{\perp}}\right)^{-1/4} \left(\frac{8R_0 q}{q' n}\right)^{1/2}. \tag{1}$$

Here, R_0 denotes the major plasma radius, n the poloidal mode number of the island, q the safety factor, and $q' = dq/dr$ its radial derivative.

The reduced pressure gradient inside magnetic islands caused by the temperature flattening perturbs the bootstrap current and gives rise to neoclassical tearing modes (NTMs). The amplitude of the driving term depends on w and w_c [2, 3]. Despite its important role for the dynamics of NTMs, which are expected to set the β-limit in the ITER conventional scenarios [4], the heat diffusion anisotropy cannot be measured directly in experiments.

In this article, we are systematically comparing experimental measurements of the temperature distribution around a magnetic island to numerical heat diffusion simulations that are performed with the methods developed in Refs. [5, 6] and are capable of treating realistic values of the heat diffusion anisotropy in toroidal geometries [7]. We present a method to determine the experimental heat diffusion anisotropy and the magnetic island size from this comparison. The application of the method is demonstrated for a $2/1$ magnetic island triggered by the dynamic ergodic divertor (DED) coil set [8] in the TEXTOR tokamak [9]. The experimental electron temperature around the island, measured by ECE-Imaging (electron cyclotron emission imaging) [10], is compared to the numerical simulation results.

2. TEXTOR Experiments

The TEXTOR discharge #99175, which is characterised by a magnetic field strength of 2.25T and a plasma current of about 300kA, is studied. TEXTOR is a limiter tokamak with a circular plasma cross-section [9]. At the time considered (around $t = 1.6$s), the plasma is heated by roughly 250kW of Ohmic (OH) heating and about 300kW of neutral beam injection (NBI) heating. The volume-averaged value of the normalised plasma beta,

$$\beta_N = \beta_t[\%]\frac{a[\mathrm{m}]B_t[\mathrm{T}]}{I_p[\mathrm{MA}]}, \tag{2}$$

takes a value of about 0.3. Here, $\beta_t = 2\mu_0 < p > /B_t^2$ denotes the volume averaged toroidal plasma beta, a the minor plasma radius, B_t the toroidal magnetic field strength, I_p the total plasma current, μ_0 the magnetic constant, and $< p >$ the volume averaged pressure. An overview over the most important plasma parameters is given in Fig. 1.

2.1. Magnetic Perturbation Profiles

TEXTOR is equipped with a set of 16 helical perturbation field coils of the dynamic ergodic divertor (DED). The principal component of the perturbation field that can be produced by these coils may be varied between $3/1$, $12/4$, and $6/2$ operation. In our case, the $3/1$ configuration is used with a 1kHz AC current which gives rise to a magnetic perturbation that rotates around the torus. The amplitude of the coil currents is ramped up from 0kA to 1.9kA between $t \approx 1.22$s and 1.74s. The magnetic perturbation has a strong $2/1$ sideband that gives rise to a rotating $2/1$ magnetic island. As the DED coil currents act just as an additional driving term in the Rutherford equation that determines the magnetic island dynamics, DED-islands are not different from "usual" magnetic islands.

The considered island starts to grow at about $t = 1.55$s and locks to the external perturbation field at $t = 1.58$s. Our comparison will be performed during the island growth phase after the mode has locked. The radial profiles of the $2/1$ magnetic perturbation required for our calculations are derived from nonlinear cylindrical two-fluid MHD simulations. These are performed for typical TEXTOR parameters analogous to Ref. [11] and do not rely on the so-called vacuum assumption but include the full plasma interaction with the external magnetic perturbation. The obtained profiles are depicted in Fig. 2 for two different perturbation amplitudes that lead to different island sizes. Only the $2/1$ magnetic perturbation excited by the DED coils is taken into account in our simulations. By performing vacuum magnetic field calculations, we have checked that the full DED spectrum does not lead to a significant stochastisation at the island separatrix in our case such that the assumption can not affect the obtained results for the heat diffusion anisotropy.

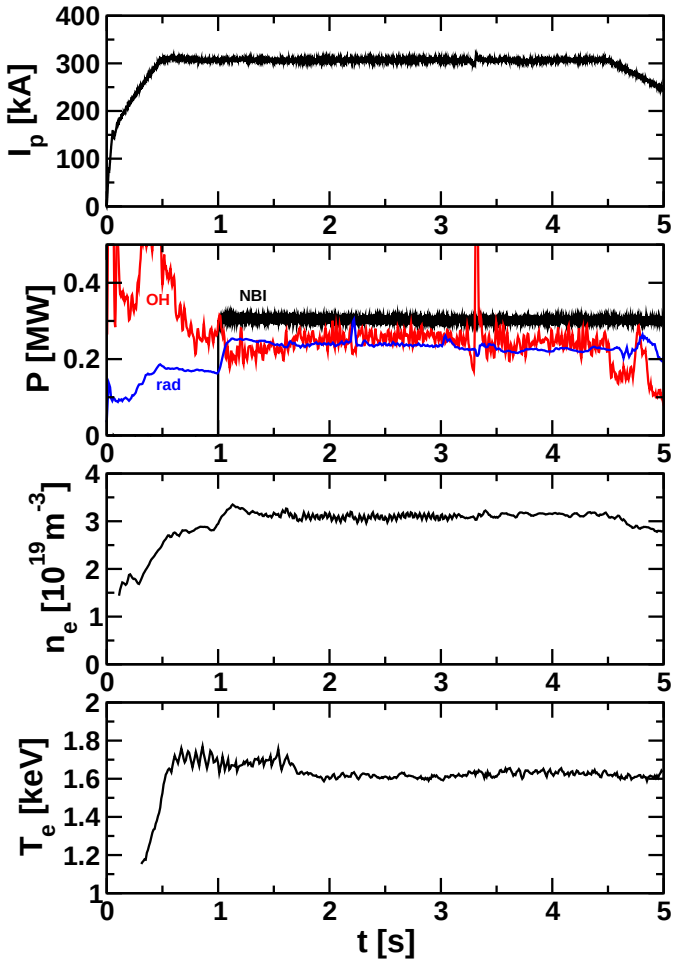

Figure 1: The most important plasma parameters of TEXTOR discharge #99175 are shown. From top to bottom, time-traces of the total plasma current, the heat source and drain powers (Ohmic, NBI, and radiated), the core electron density, and the core electron temperature are given. The local electron density is reconstructed from the line-integrated values measured with HCN interferometry along many lines of sight.

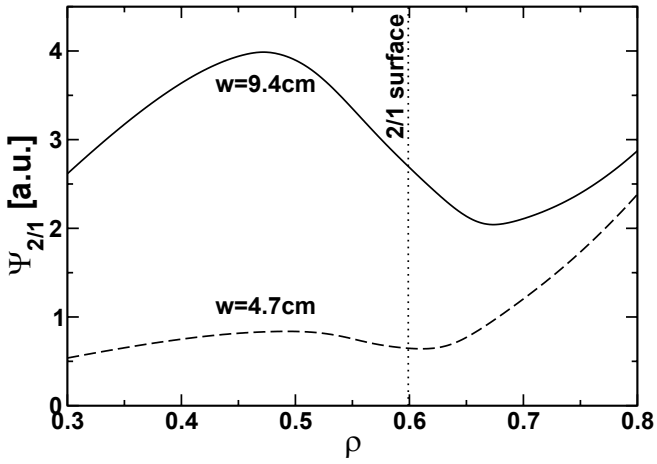

Figure 2: Radial profiles of the $^2/_1$ magnetic perturbation are shown for two different perturbation amplitudes that lead to island sizes of 4.7cm respectively 9.4cm.

2.2. Temperature Measurements

The electron temperature around the island is measured by TEXTOR's ECE-Imaging diagnostic [10] that consists of an array of 8 radial times 16 vertical channels, which are located around the outer mid-plane for this shot. Thermal noise intrinsic to any ECE measurement is suppressed by applying singular value decomposition (SVD) to the measured data array and keeping the 10 most significant eigenvector pairs. The incoherent data can be removed this way allowing to resolve temperature fluctuations of small scales and amplitudes. SVD still ensures that the statistics of all 128 channels enter into the noise suppression although only some of the channels are actually used for the comparison.

The average electron temperature within a volume of roughly 1cm^3 is measured by every ECE-Imaging channel. Assuming rigid body rotation, the time-trace of each channel provides data corresponding to a toroidal temperature profile at a different radial position in the vicinity of the $^2/_1$ resonant surface. From the channels that are located at $Z = 0$, six were selected that are situated sufficiently close to the $^2/_1$ resonant surface to be relevant for our comparison. The channels, which will be referred to as $E_1 \ldots E_6$ in the following, are located between $R = 2.05$m and 2.10m. The measurements determine the temperature distribution at the magnetic island on the low-field side of the plasma. For an island width of 8cm, the position of the channels relative to the island is illustrated in Fig. 3. The spatial resolutions of the ECE-Imaging measurement in radial and vertical directions are determined by the distance of the individual ECE-Imaging channels and by the size of the volume over which each channel "averages" the temperature. Both length scales are about one centimetre. The measurement was carried out with a sample frequency of 200kHz and down-sampled to 100kHz. This results in about 100 data points per mode transit around the torus which corresponds to a toroidal resolution of about 11cm.

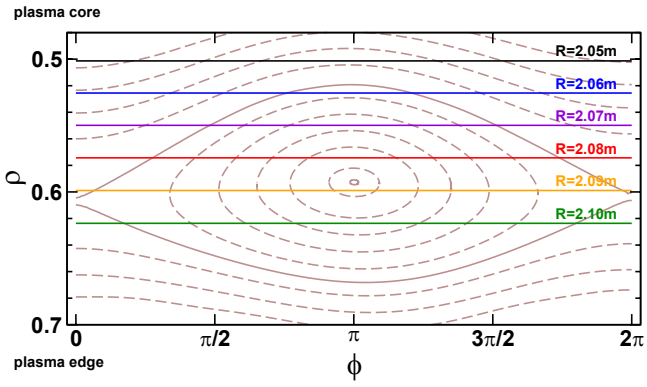

Figure 3: For the reconstructed magnetic field topology at $t = 1.598$s with an 8cm wide $2/1$ island, a Poincaré plot that displays the magnetic flux surfaces is shown together with the lines along which the temperature is measured by the six ECE-Imaging channels at $R = 2.05$m, 2.06m, …, 2.10m.

The ECE-Imaging signals are first cross-calibrated against the 1D ECE diagnostic. Successively, a careful relative calibration between the channels is performed that is determined using the measurements at a large magnetic island, where the temperature inside the island is known (e.g. from the time-traces of the ECE-Imaging signals) to be largely flattened. The calibration is kept fixed for all cases considered. The experimental data is cut into time-fragments that correspond to one mode-transit around the torus, each (X-point to X-point of the island). These segments will be compared to numerical simulations later on.

3. Physics Model

The island evolution is slow enough such that the temperature distribution can be assumed to follow changes of the magnetic topology instantaneously. We therefore model the electron heat transport by the steady-state anisotropic heat diffusion equation,

$$\nabla \cdot \mathbf{q}_e = P_e, \tag{3}$$

where

$$\mathbf{q}_e = -n_e \left[\chi_{||,e} \nabla_{||} T_e + \chi_{\perp,e} \nabla_{\perp} T_e \right] \tag{4}$$

is the electron heat flux density, n_e denotes the electron particle density, T_e the electron temperature, P_e the electron energy source (and sink) term, $\nabla_{||} T_e = \hat{\mathbf{b}}(\hat{\mathbf{b}} \cdot \nabla T_e)$ the temperature gradient parallel to the magnetic field lines, $\nabla_{\perp} T_e = \nabla T_e - \nabla_{||} T_e$ the cross-field temperature gradient, and $\hat{\mathbf{b}} = \mathbf{B}/B$ the magnetic field direction vector.

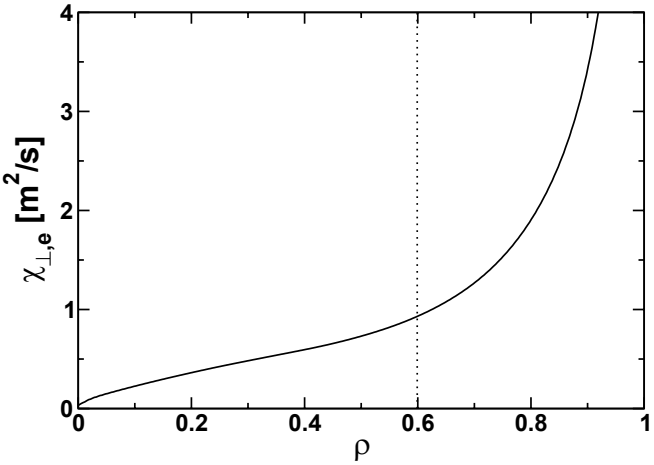

Figure 4: The profile of the unperturbed cross-field heat diffusion coefficient, $\chi_{\perp,e}$, is given. It is determined by a numerical simulation from the unperturbed temperature profile prior to the mode onset and the heat deposition profile.

The local heating power density at the magnetic island does not play an important role for our investigations as the temperature distribution is not peaked significantly around the O-point of the island. We assume that the electrons are effectively heated by half of the sum of Ohmic and NBI heating powers. Radiative losses that probably originate mostly from carbon ions at the plasma boundary are neglected. Moderate inaccuracies in the heating power density can not affect the obtained value of the heat diffusion anisotropy but only the profile of the cross-field diffusivity which leads, in turn, only to a marginal error in the calculation of the analytic anisotropy predictions that we are comparing to. This error may be neglected as it is much smaller than the uncertainty of the heat diffusion anisotropy obtained from the comparison between measured and simulated temperature profiles.

The profile of the unperturbed cross-field heat diffusion coefficient, $\chi_{\perp,e}$, can be determined from the heating power deposition profile and the temperature profile measured prior to the onset of the magnetic island. The resulting profile is plotted in Fig. 4 and is used for the successive simulations. At the $2/1$ resonant surface, $\chi_{\perp,e}$ takes a value of about $0.9\mathrm{m}^2/\mathrm{s}$. We assume that the island does not alter the profile significantly. Inside magnetic islands, the perpendicular heat diffusion coefficient may, however, be different from its value outside the island [12, 13]. The value of $\chi_{\perp,e}$ inside the island influences how strongly the temperature peaks around the O-point due to local heat sources. In the considered TEXTOR discharge, the small amount of local Ohmic and NBI heating inside the magnetic island leads only to a very moderate peaking. Comparing it to the simulations indicates a cross-field diffusivity inside the island that is of a similar order as outside the island. However, the uncertainties due to the low local heating powers do not allow to investigate this issue in more detail. Examinations with electron cyclotron resonance heating into the magnetic island are planned to be considered for this purpose.

Our computations are performed with the 3D finite difference scheme developed in Ref. [5] that is capable of treating realistic values of the heat diffusion anisotropy without the requirement of a full coordinate alignment to the magnetic field lines and has already been applied to toroidal geometries [7]. The coordinate system chosen is an unsheared helical straight field line coordinate system whose helicity is aligned to the $2/1$ magnetic island to reduce the necessary toroidal resolution. The radial, poloidal and toroidal coordinates are denoted ρ, θ, and ϕ. For details on the tensorial form of the heat diffusion equation and the helical coordinate system, readers may refer to Sections II.B and II.E of Ref. [7].

4. Comparison between simulations and measurements

Our method is now applied to TEXTOR discharge number 99175. Equipped with the profiles for the heating power density, the electron density, the magnetic perturbation, and the equilibrium cross-field heat diffusivity, Eqs. (3) and (4) are solved for various values of island width and heat diffusion anisotropy:

$$\begin{aligned} w &= 4.0\text{cm},\ 4.5\text{cm},\ \ldots,\ 11.0\text{cm} \\ \chi_{||}/\chi_{\perp} &= 1\cdot 10^7,\ 1.5\cdot 10^7,\ 2\cdot 10^7,\ 3\cdot 10^7,\ 5\cdot 10^7,\ 7\cdot 10^7,\ 1\cdot 10^8,\ \ldots,\ 1\cdot 10^9 \end{aligned}$$

The simulations were carried out with 91 radial, 129 poloidal and 17 toroidal grid points. The radial range between $r/a = 0.35$ and $r/a = 0.8$ was resolved, where r denotes the local minor radius and a the minor plasma radius. For each mode-transit, the numerical simulation is selected that reproduces the experimental temperature measurements best as indicated by the smallest quadratic deviations. The matching algorithm is described in detail in Appendix A.

"Numerical temperature signals", separated by $\Delta R = 0.25$cm, are determined as toroidal profiles ($\phi = 0 \ldots 2\pi$) at the outer mid-plane ($Z = 0$). As the distance between the ECE-Imaging channels is approximately 1cm, every fourth numerical signal has to be compared to an experimental channel. An integer number i is introduced, such that the numerical signals $N_i, N_{i+4}, \ldots, N_{i+20}$ are matched to the experimental channels $E_1, E_2, \ldots, E_6$. The most reasonable value for i is selected automatically in every matching procedure to account for a possible slight variation of the safety factor profile due to the growing magnetic island. For the considered discharge, i stays virtually constant which corresponds to a fixed mapping between experimental channels and numerical signals and indicates that the position of the $2/1$ resonant surface does not vary by more than 0.5cm.

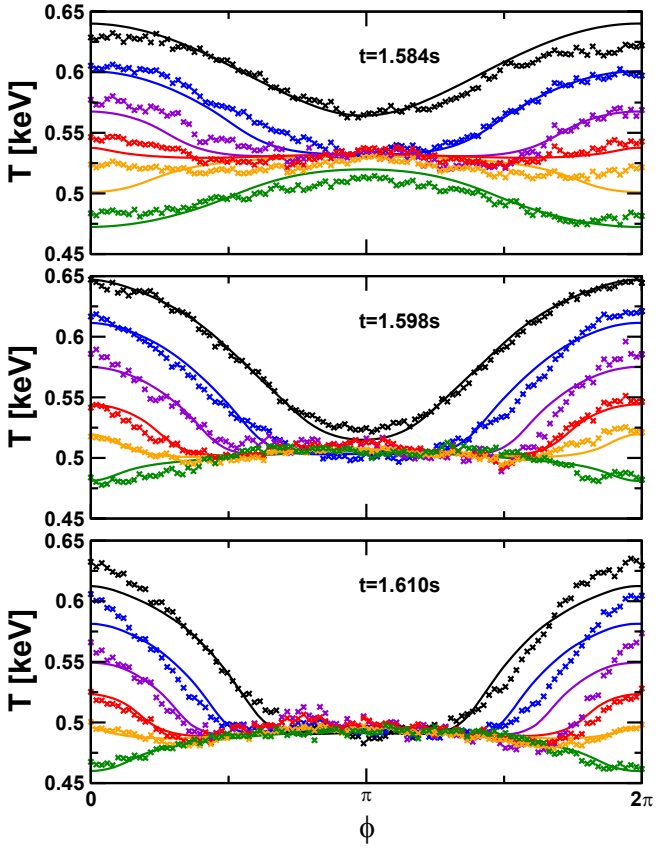

Figure 5: Comparisons of experimental temperature measurements ("×") to numerical simulation results (solid lines) for three different times. The island X-point is located at $\phi = 0$ and $\phi = 2\pi$ while the O-point is positioned at $\phi = \pi$.

4.1. Matching of measured and calculated temperature profiles

For $t = 1.598$s, Fig. 3 shows a Poincaré plot of the reconstructed magnetic field structure together with the lines along which the temperature is measured by the six considered ECE-Imaging channels. Very good agreement between numerical simulations and experimental data is obtained in the considered time-interval between $t = 1.584$s and 1.610s. For three representative time-points, the experimental and numerical data sets are compared in Fig. 5. The deviation seen around the X-point at $t = 1.584$s is probably caused by two factors. Firstly, the distance between the ECE-Imaging channels is not exactly 1cm as assumed for our comparison, but varies between 0.9cm and 1.2cm. Secondly, the calculations are performed in steps of $\Delta w = 0.5$cm for the magnetic island size, only, which are quite large at small magnetic islands.

The time-trace of the matching error, i.e., the quadratic difference between the measured and calculated temperature profiles, is plotted in Figure 6. For the determination of $\chi_{||}/\chi_{\perp}$, the

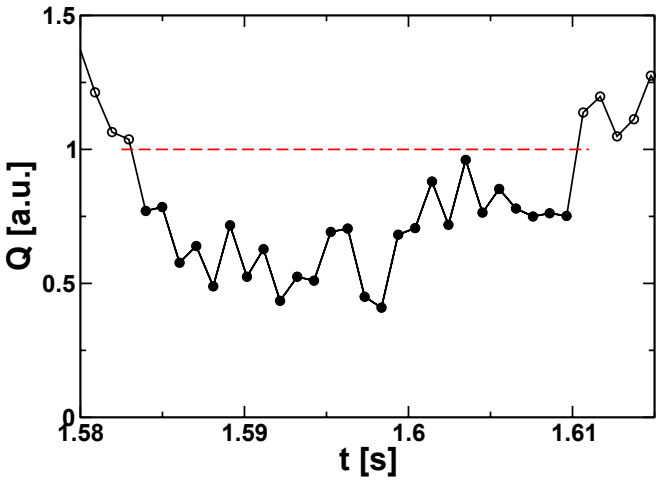

Figure 6: The quadratic differences, Q, between experimental measurements and numerical simulations are given for each mode-transit. We consider $t = 1.584 \ldots 1.610$s for the determination of the heat diffusion anisotropy.

time-interval between $t = 1.584$s and 1.610s is used where the numerical simulations are able to reproduce the experimental measurements very accurately. The strongly increased error prior to this time-interval originates from distinct irregularities in the ECE-Imaging signals. These probably arise as the island is not yet locked completely to the external perturbation field and fluctuates between locking and unlocking. After $t = 1.61$s, the island has become larger than 20 percent of the minor radius. Higher harmonic magnetic perturbations ($1/1$, $3/1$, $3/2$, $5/2$, ...), that are excited due to toroidicity, arise in the simulations at this point and start to cause stochastisation of the island separatrix. It is, however, not clear if this stochastisation is also present in the experiment. The temporal resolution of CXRS (charge exchange recombination spectroscopy) measurements is not sufficient to tell if the plasma is still rotating differentially at the time of interest right after the $2/1$ mode locking or if the differential rotation has already vanished. In case of differential rotation, the higher harmonics would not be coupled and the stochastisation removed by shielding currents.

4.2. Sensitivity of the simulated temperature signals on w and $\chi_{||}/\chi_{\perp}$

In the following, the sensitivity of the simulated temperature signals on variations of the island width and the heat diffusion anisotropy will be demonstrated. This allows to give an estimate for the accuracy of the values determined by the matching procedure between experimental and numerical data. For this purpose, results for $t = 1.598$s will be analysed in detail, where an island width of 8.0cm and a heat diffusion anisotropy of $\chi_{||}/\chi_{\perp} = 1 \cdot 10^8$ are detected.

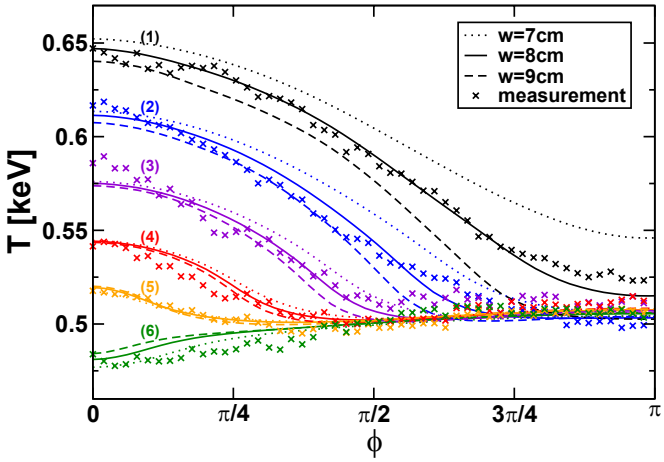

Figure 7: The sensitivity of the temperature signals on the island width is shown for $t = 1.598$s with $\chi_{||}/\chi_{\perp} = 1 \cdot 10^8$. For this purpose, temperature signals for $w = 7$cm (dotted lines), 8cm (solid lines), and 9cm (dashed lines) are compared. Only the temperature signals far from the resonant surface are affected significantly by small changes of the island width. For this case, an island width of about 8cm is required in the simulation to reproduce the measured temperature distribution.

As seen from Fig. 7, the numerical temperature signals close to the resonant surface (numbered (4), (5), and (6) in Fig. 7) remain virtually unchanged, if the island width changes from 8cm to 7cm respectively 9cm. In contrast, temperature signals far from the resonant surface (e.g., number (1) in Fig. 7) are affected very strongly. The measured temperature distribution is not reproduced reasonably by simulations with island widths of 7 respectively 9cm, but very well by $w = 8$cm. The detected island widths are therefore reliable to ± 0.5cm.

As expected, the heat diffusion anisotropy affects the temperature signals far from the resonant surface only slightly except for some offset shift. However, the signals close to the resonant surface are changed quite significantly in the X-point region ($\phi \approx 0$), as seen from Fig. 8. Clearly, the computations performed for $\chi_{||}/\chi_{\perp} = 2 \cdot 10^7$ and $\chi_{||}/\chi_{\perp} = 5 \cdot 10^8$ reproduce the measured temperature distribution much worse than the simulation with $\chi_{||}/\chi_{\perp} = 1 \cdot 10^8$. The detected values of the heat diffusion anisotropy for each mode-transit around the torus are therefore reliable to a factor smaller than 5.

4.3. Results

The matching procedure explained in the previous Subsection is now applied to the temperature measurements of many mode transits around the torus. Thus, time-traces of the island width

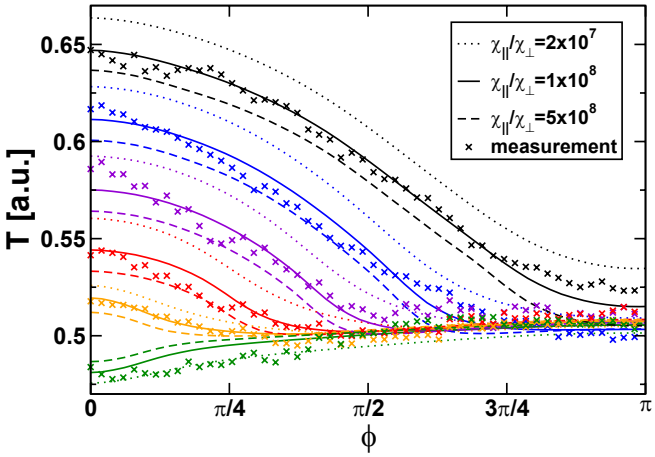

Figure 8: The dependence of the temperature signals on the heat diffusion anisotropy is shown. For this purpose, temperature signals for $\chi_{||}/\chi_{\perp} = 2 \cdot 10^7$ (dotted lines), $1 \cdot 10^8$ (solid lines), and $5 \cdot 10^8$ (dashed lines) are compared. The value of $\chi_{||}/\chi_{\perp}$ mostly affects the temperature distribution around the X-point (green, orange and red curves around $\phi = 0$). For the considered mode-transit at $t = 1.598$s, a heat diffusion anisotropy around $1 \cdot 10^8$ is required to reproduce the measured temperature signals numerically.

and the heat diffusion anisotropy are obtained. From Figure 9, the magnetic island width can be seen to increase from about (5.5 ± 0.5)cm to (9.5 ± 0.5)cm within the considered time-interval of 26ms which corresponds to a growth rate of about (1.5 ± 0.3)m/s. The heat diffusion anisotropy fluctuates around a value of about 10^8. This corresponds to a value of the critical island width for temperature flattening, w_c, equal to about 2cm. Thus, the value of w/w_c, changes roughly from 3 to 5.

The distribution of the obtained values for $\chi_{||}/\chi_{\perp}$ is analysed in Figure 10. It is seen to agree quite well with a Gaussian distribution which allows to approximate the statistical uncertainty. We obtain $\chi_{||}/\chi_{\perp} \approx 8 \cdot 10^7$ with an uncertainty factor of about 2. Due to the large number of "measurements" of the heat diffusion anisotropy, the uncertainty is significantly smaller than that of one single mode-transit which was estimated in Section 4.2. The assumed systematical error of 30 percent in the value of $dq/d\rho$ at the $^2/_1$ resonant surface results in an additional factor of 2. Altogether, the observed heat diffusion anisotropy at the considered $^2/_1$ magnetic island is

$$\chi_{||}/\chi_{\perp} = 10^{7.9 \pm 0.5}. \tag{5}$$

4.4. Discussion

In a typical tokamak plasma, the temperature gets constant on flux surfaces irrespective of the exact value of the heat diffusion anisotropy except for those surfaces that belong to the heat

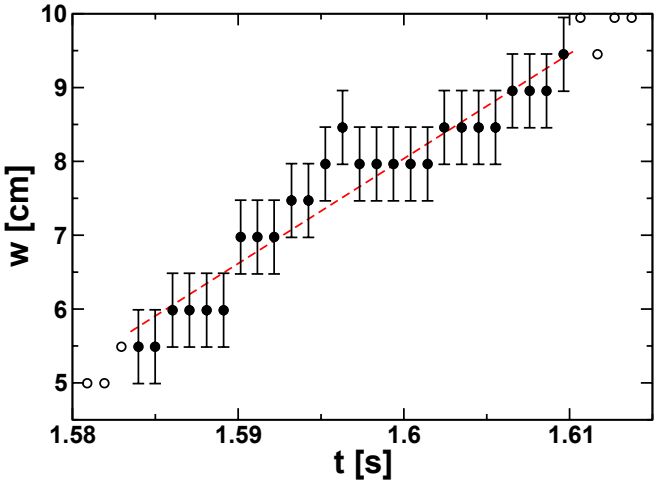

Figure 9: The evolution of the island size is shown. The island width grows from about 5.5cm to 9.5cm during the considered time-interval.

conduction layer of a magnetic island which is located at the island's separatrix [2]. Only in this region, the temperature distribution is sensitive to the heat diffusion anisotropy. It is consequently the effective heat diffusion anisotropy of the heat conduction layer that we determine by our comparison.

Spitzer and Härm derived the expression

$$\chi_{||}^{SH} = 3.16 \cdot v_{th,e} \cdot \lambda_e \approx 3.6 \cdot 10^{29} \frac{T_e[\mathrm{keV}]^{5/2}}{n_e[\mathrm{m}^{-3}]} \mathrm{m}^2/\mathrm{s} \tag{6}$$

for the parallel heat diffusivity assuming free-streaming electrons, where $v_{th,e}$ denotes the electron thermal velocity, λ_e the collisional electron mean free path, T_e the electron temperature given in keV, and n_e the electron density given in m^{-3} [1, 14]. According to the Spitzer-Härm formula, a heat diffusion anisotropy around $4 \cdot 10^9$ would be expected at the considered $^2/_1$ island in TEXTOR. In the calculation of this prediction, the cross-field diffusivity of Fig. 4 enters. This seems to be reasonable as we do not see an indication for a considerably different cross-field diffusivity inside the island as discussed in Section 3. Additionally, the cross-field diffusivity is relevant only in the heat conduction layer around the island separatrix and not further inside the island. A deviation of the cross-field diffusivity from the value of the background plasma can generally not affect the value obtained for the heat diffusion anisotropy by comparing experiment and simulation, but only the calculation of the Spitzer-Härm prediction. A reduced cross field diffusivity would lead to an even higher anisotropy prediction such that the qualitative conclusion of this work would not be altered.

The temperature at the magnetic island changes by 8 percent in the considered time-interval which corresponds to a change of the anisotropy prediction of about 20 percent which is negli-

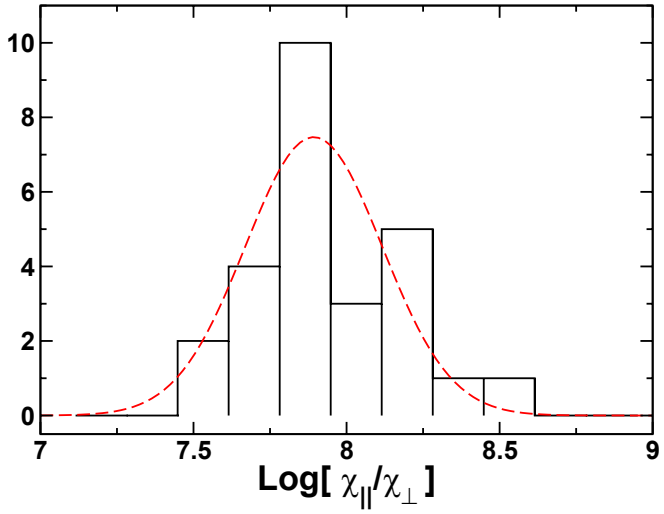

Figure 10: The obtained values for the heat diffusion anisotropy roughly form a Gaussian distribution (dashed line). This allows to estimate the statistical uncertainty of the obtained values.

gible. Inaccuracies in the perpendicular heat diffusion coefficient caused by uncertainties in the electron heating power profile may affect the calculated anisotropy prediction only slightly and can be neglected as well.

The predicted heat diffusion anisotropy is by a factor of roughly 40 higher than what we observe which is an indication for the so-called heat flux limit, first derived by Malone, McCrory and Morse [15]. It predicts the same heat diffusion anisotropy as Spitzer and Härm in a very thin layer ($\lesssim$ 1mm) around resonant surfaces and the separatrices of magnetic islands, but values reduced by 1 or 2 orders of magnitude apart from these. An indication for the heat flux limit has previously also been found by Tokar and Gupta using an analytical approach [16].

In the considered discharge, the width of the heat conduction layer around the $^2/_1$ island is roughly between 0.5cm and 2cm according to the analytical estimate given in Ref. [2]. Thus, the heat diffusion anisotropy is predicted to be much lower than the Spitzer-Härm level over most of the heat conduction layer according to heat flux limit theory. Qualitatively, this prediction agrees very well with our observation that the effective heat diffusion anisotropy in the heat conduction layer is much lower than the Spitzer-Härm level.

5. Summary

A method for the determination of the magnetic island size and the heat conduction anisotropy in the experiment by comparing results of numerical heat diffusion computations to experimental temperature measurements has been developed. An algorithm automatically detects the numerical temperature profiles across a magnetic island that reproduces the measurements for every mode transit around the torus best. As the heat diffusion anisotropy is a key parameter for the understanding of neoclassical tearing modes but cannot be measured directly in the experiment, the demonstrated method might help to improve the understanding of island dynamics.

The scheme has been applied to a $^2/_1$ magnetic island in the TEXTOR tokamak that grows from about $w = 5.5\text{cm}$ to 9.5cm at a growth rate of $1.5\text{m}/\text{s}$. The ratio between the island width, w, and the scale island width for temperature flattening, w_c, changes, accordingly, from 3 to 5. A heat diffusion anisotropy of 10^8 is observed with an uncertainty factor of 3. This is lower than the Spitzer-Härm prediction by a factor of roughly 40 and strongly supports the heat flux limit theories. The method is also planned to be applied to neoclassical tearing modes in ASDEX Upgrade.

A. Automatic Matching of Experimental and Numerical Data

For every matching attempt between the measurements of a mode-transit and a numerical computation, the quadratic differences between numerical signals $N_i, N_{i+4}, \ldots N_{i+20}$ and experimental channels $E_1, E_2, \ldots E_6$ are pair-wisely integrated over the full transit ($\phi = 0 \ldots 2\pi$) giving the quadratic differences $Q_1 \ldots Q_6$ of the channel-pairs. The total quadratic difference between the measured mode-transit and the numerical simulation is then given by $Q = \sum_{k=1\ldots6} Q_k$. The small deviations between the average experimental and numerical temperatures resulting from fluctuations in the experiment are removed prior to the determination of the quadratic differences. The relative calibration of the channels is naturally not altered by this procedure and remains unchanged during the whole comparison.

The most reasonable value for the index i that determines which numerical signals are matched to the experimental channels is chosen for any combination of an experimental measurement and a numerical computation by minimising Q. Then, for every mode-transit, again by minimising Q, the numerical computation is selected that reproduces the measured temperature distribution best. This way, an estimate for w and $\chi_{||}/\chi_{\perp}$ is obtained, for each mode-transit independently. In summary, the algorithm given in pseudo-code is as follows:

```
for every measured mode-transit, do
    for every numerical computation, do
        for every value of i, do
            Determine the quadratic difference Q
            between measurement and simulation.
        done;
        Select the value for i with minimal Q.
    done;
    Select the numerical simulation with minimal Q.
done;
```

Pseudo-code is a compact and informal high-level description of an algorithm. It may use the structural conventions of some programming language, but is intended for human reading. The description is independent of the programming language it will be implemented in.

References

[1] L. Spitzer and R. Härm. Phys. Rev. **89**, 997 (1953).

[2] R. Fitzpatrick. Phys. Plasmas **2**, 825 (1995).

[3] M. Hölzl, S. Günter, Q. Yu, and K. Lackner. Phys. Plasmas **14**, 052501 (2007).

[4] ITER Physics Basis Editors, ITER Physics Expert Group Chairs and Co-Chairs, ITER Joint Central Team, and Physics Integration Unit. Nucl. Fusion **39**, 2137 (1999).

[5] S. Günter, Q. Yu, J. Krüger, and K. Lackner. J. Comput. Phys. **209**, 354 (2005).

[6] S. Günter, K. Lackner, and C. Tichmann. J. Comput. Phys. **226**, 2306 (2007).

[7] M. Hölzl, S. Günter, and ASDEX Upgrade Team. Phys. Plasmas **15**, 072514 (2008).

[8] Fusion Eng. Design, edited by K. H. Finken, volume 37, Issue 3 (Special Issue), pages 335–448 (1997).

[9] U. Samm. Fusion Sci. Technol. **47**, 73 (2005).

[10] H. Park, C. C. Chang, B. H. Deng, , C. W. Domier, A. J. H. Donné, K. Kawahata, C. Liang, X. P. Liang, H. J. Lu, , N. C. Luhmann, Jr., A. Mase, H. Matsuura, E. Mazzucato, A. Miura, K. Mizuno, T. Munsat, Y. Nagayama, M. J. van de Pol, J. Wang, Z. G. Xia, and W.-K. Zhang. Rev. Sci. Instrum. **74**, 4239 (2003).

[11] Q. Yu, S. Günter, and K. H. Finken. Phys. Plasmas **16**, 042301 (2009).

[12] S. Inagaki, N. Tamura, K. Ida, Y. Nagayama, K. Kawahata, S. Sudo, T.Morisaki, K. Tanaka, T. Tokuzawa, and LHD Experimental Group. Phys. Rev. Lett **92**, 055002 (2004).

[13] G. Spakman, G. Hogeweij, R. Jaspers, F. Schüller, E. Westerhof, J. Boom, I. Classen, E. Delabie, C. Domier, A. Donné, M. Kantor, A. Krämer-Flecken, Y. Liang, N. L. Jr, H. Park, M. van de Pol, O. Schmitz, J. Oosterbeek, and the TEXTOR Team. Nucl. Fusion **48**, 115005 (2008).

[14] S. I. Braginskii. Reviews of Plasma Physics, volume 1, pages 205–311. Consultants Bureau, New York (1965).

[15] R. C. Malone, R. L. McCrory, and R. L. Morse. Phys. Rev. Lett. **34**, 721 (1975).

[16] M. Z. Tokar and A. Gupta. Phys. Rev. Lett. **99**, 225001 (2007).